DFT investigation of 2-mercaptobenzothiazole adsorption on model oxidized copper surfaces and relationship with corrosion inhibition

Fatah Chiter, Dominique Costa, Vincent Maurice, Philippe Marcus

DFT investigation of 2-mercaptobenzothiazole adsorption on model oxidized copper surfaces and relationship with corrosion inhibition

Fatah Chiter*, Dominique Costa**, Vincent Maurice, Philippe Marcus

PSL Research University, CNRS – Chimie ParisTech, Institut de Recherche de Chimie Paris (IRCP), Physical Chemistry of Surfaces Group, 11 rue Pierre et Marie Curie, 75005 Paris, France

Abstract

2-mercaptobenzothiazole (MBT) is known as an efficient corrosion inhibitor for copper. In the present work, we performed quantum chemical DFT calculations of the interaction of MBT on Cu(111) surfaces covered by an ultrathin Cu_2O(111) film, in order to bring atomic scale insight on the corrosion inhibition properties of MBT on oxidized copper surfaces. Thione and thiolate forms of MBT are found to interact strongly with the oxidized surfaces. The formation of a monolayer at full coverage is favored over single molecular adsorption at low coverage with the molecules adopting a perpendicular orientation. Thione binds strongly via covalent bonding between the exocyclic sulfur atom and the under coordinated Cu site, and additional H-bonding between the NH group and surface oxygen atoms (NH...O H-bond). Thiolate binds more strongly via a second covalent bond between the N atom and saturated Cu site. Bonding interaction is confirmed by the electronic structure analysis and charge transfer. The adsorption process leads to the reconstruction of the topmost oxide surface. The calculations suggest that both forms of MBT may substitute H_2O and OH at the Cu_2O film surface, and thus may form a protective layer on oxidized copper surfaces in aqueous environment.

Keywords: 2-mercaptobenzothiazole, Copper, Oxide, Corrosion, Organic inhibitor, DFT

*Corresponding author: fatah.chiter@chimieparistech.psl.eu

**Corresponding author: dominique.costa@chimieparistech.psl.eu

1. Introduction

Corrosion of metals and alloys is an ubiquitous phenomenon with huge economic impact, which affects many industrial sectors. Its prevention is thus a crucial issue. One of the solutions to mitigate corrosion is the use of organic corrosion inhibitors [1, 2, 3], that are considered as promising candidates to replace chromate-based coatings [4, 5, 6]. Various organic compounds containing nitrogen, oxygen and sulfur heteroatoms, polar functional groups, and conjugated double bonds are used to prevent the corrosion of copper [7, 8, 9, 10, 11, 12, 13, 14].

Among these organic molecules, 2-mercaptobenzothiazole (MBT) has been shown to improve the corrosion resistance of copper in various conditions. Indeed, MBT exhibits different active sites and may have different types of interaction with the surface (H-bonding, electrostatic, covalent bonding). Still, the question of the detailed interaction and monolayer formation of MBT in its various forms (thiol, thione, anionic) on copper surfaces in metallic or oxidized or passivated states, remains opened.

Several experimental works showed that MBT exhibits corrosion inhibition efficiency on copper. Chadwick and Hashemi [15] studied the corrosion inhibition of copper by MBT and MBI (2-mercaptobenzoimidazole) in different experimental conditions (pH, immersion time and presence of Cl and copper ions) using X-ray photoelectron spectroscopy (XPS) and X-ray induced Auger spectroscopy (X-AES). They found that the formation of a Cu-MBT film is possible under all conditions and that the organic film thickness depends on the pH of the treatment solution, which reflects the stability and thickness of the Cu_2O passivating surface oxide. In the Cu_2O stability domain (pH>4), the thickness of organic films cannot exceed the monolayer without copper ions in the solution, whereas, in the Cu_2O instability domain (pH<3), the thickness of the organic film may be increased to any desired value. Ohsawa and Suetaka [16] used various spectroscopy techniques in order to clarify the mechanism of corrosion inhibition of Cu by MBT and showed the formation of a surface film that acts as barrier isolating the metal from the corrosive media. The mechanism would consist of the surface reaction of cuprous ions with adsorbed MBT and not of a complex precipitated from bulk solution and involving the ionized thiol form and copper ions in ethanol solution [17]. Because corrosion processes are highly sensitive to pH,

Ramírez-Cano et al. [18] imaged in situ the pH distributions produced in the surrounding electrolyte by the interaction of MBT with copper by using scanning electrochemical microscopy (SECM) in potentiometric mode. They concluded that the presence of an adsorbed MBT film on Cu shifts the pH towards more alkaline values in a small volume of NaCl solution.

Some studies also investigated the adsorption sites and film formation in different experimental conditions. Finšgar and Merl [19] showed using electrochemical techniques that in chloride media MBT acts as mixed-type (i.e. anodic and cathodic) inhibitor on copper. The surface layer thickness was estimated to be 1.5 ± 0.5 nm and the adsorption of the thione form (MBTH) via the N and exocyclic S atoms to Cu was concluded from XPS measurements. Kazansky et al. [20] determined similar adsorption mechanism of MBT in neutral phosphate media. However, Woods et al. [21] investigated by Surface Enhanced Raman Spectroscopy (SERS) the interaction of MBT with copper, silver and gold surfaces. They found that MBT chemisorption on all three metals involves bonding between the exocyclic S and metal atoms. They concluded using XPS, that the surface layer is of monolayer thickness. In contrast, Shahrabi et al. [22] reported that the adsorption of inhibitors (MBT, MBI and MBO) on copper in sulphuric acid solution is physical via electrostatic interaction and that no covalent bonding between inhibitor molecule and metal surface is established.

The synergistic effect of MBT with other species has been established. He et al. [23] investigated the corrosion inhibition of MBT with and without the presence of halide ions on copper in sulfuric acid solution. They concluded that the growth kinetics of the Cu-MBT film depends on the concentration of ions and that I^- promotes the synergistic formation of the protective film. Bao et al. [24] used MBT to develop antibacterial coatings, aiming to solve microbiologically influenced corrosion (MIC) problems. MBT doped chitosan/11-alkanethiolate acid composite coating was found to improve copper protection (anticorrosion and antibacterial) in NaCl solution and in the presence of sulphate reducing bacteria (SRB). Moreover, the MBT molecule inhibited both anodic and cathodic reactions [17, 18, 22, 24].

The surface state of copper has an impact on MBT adsorption. Chadwick and Hashemi [15] demonstrated the influence of the oxidation state on MBT adsorption. Kazansky et al. [20] suggested that a thin Cu_2O layer is required for the formation of the MBT layer, which thickness would depend on the immersion time in neutral phosphate media. Recently, Chen and Erbe. [25] reported using in situ infrared and Raman spectroscopy that in reducing con-

ditions in alkaline electrolyte, MBT forms a monolayer on the oxide free Cu surface and prevents oxide formation. The inhibiting effect of a pre-adsorbed monolayer of MBT on oxide fomation is also found from studies of adsorption from the gas phase on surfaces prepared in well-controlled conditions under ultra low pressure [26, 27]. Thus, it appears that the oxidation state of the Cu surface (metallic or covered by an oxide layer) is a determining factor in the interaction of MBT with copper.

MBT also interacts with other metal and metallic alloy surfaces and can be used for the protection against corrosion of aluminum and its alloys [28, 29, 30, 31, 32, 33, 34], steel [35, 36, 37, 38, 39, 40], brass [41, 42] and nanocomposite [43]. Others studies investigated the corrosion and lubrication properties of MBT on bronze [44] and self-healing coatings properties on magnesium and its alloys [45, 46]. The adsorption geometries of MBT monolayers on zinc [47], silver [21, 48, 47] and gold [21, 49, 50, 51] surfaces and gold nanoparticules (AuNPs) [52] were also investigated by various experimental techniques.

Thus, although corrosion inhibition is well established, the adsorption mechanisms of MBT, including the role of the surface oxide, are still subject to discussion and theoretical calculations are missing to clarify the MBT-copper interaction. Quantum calculations approach can help us to understand how inhibitors build up protective barriers against corrosion by investigating the interaction mechanisms on metallic and oxidized surfaces at the atomic and sub-atomic scales.

Very few quantum chemical studies adressed the MBT molecule and its adsorption. Theoretical calculations of the molecular properties showed that the molecule can exist in different forms in solution [39] and suggested that the thione form is a better inhibitor for steel than the thiol form. Cen et al. [35] proposed that MBT adsorbs via N and exocyclic S atoms on carbon steel (Fe). The combined first-principles and experimental study of Zhang et al. [53] showed that MBT is more able to protect Cu(220) and not able to protect Cu(200) and Cu(111) surfaces in the metallic state at low Cl concentration. MBT was found to adsorb via physical bonding on Cu(200) and Cu(111), while it chemically bonds via two sulfur atoms on Cu(220). The highest chemical activation of the (220) face would drive the better anti-corrosive ability than on the (200) and (111) faces. Vernack et al. [54] studied MBT (thiol, thione, thiolate) adsorption on Cu(111) surfaces in the metallic state. They found that the most stable configuration is that of a monolayer of the thiolate form in a perpendicular orientation and adopting a

($\sqrt{7} \times \sqrt{7}$) R19° superstructure, the molecules being bonded to the Cu atoms via the exocyclic S atoms on Cu(111) surface. Bonding to Cu atoms via the S atoms was confirmed by an experimental study of the adsorption of MBT from the gas phase on oxide-free Cu(111) surfaces controlled at the atomic scale [26, 27].

From the examination of literature data, it thus appears that the adsorption of organic inhibitors on metal and alloy surfaces and the formation of protecting layers is well established. The affinity of MBT with the metallic Cu surface has been clearly demonstrated by experimental [26, 27, 25] and theoretical [54] data. However, to the best of our knowledge, no theoretical studies of MBT adsorption on oxidized copper surfaces has been performed to complement the experimental knowledge. Indeed, depending on pH and potential, the Cu surface will be oxidized or reduced [55].

Here we report a Density Functional Theory (DFT) study of the adsorption of MBT on an oxidized Cu surface. Modeling a metal surface covered by a ultrathin oxide layer is a challenging task. Most often, the strategy is either to use a metal surface covered by an oxygen or water overlayer, or the termination of a bulk oxide. On Cu(111), Gharachorlou et al. [56] modeled one monolayer of Cu_2O on the Cu surface and Park et al. [57] modeled only a mildly oxidized (p4:O/Cu(111))) copper surface, while other groups [58, 59, 60] modeled oxidized Cu surfaces by considering the termination of a Cu_2O bulk structure.

Here we use a much more realistic model for the Cu surface passivated by a surface oxide (Cu(111)||Cu_2O(111)) derived from experimental studies. In order to better understand the role of the oxide layer, two thicknesses were considered. On these models, the MBT molecule was adsorbed and the molecular coverage, molecular conformer and energies of adsorption were systematically investigated. The adsorption of MBT is compared to water and OH adsorption in order to investigate in which conditions MBT is adsorbed at the solid/liquid interface with the passivated surface.

2. Computational details

All calculations were performed in the framework of DFT with the periodic plane-wave basis set code VASP (Vienna Ab initio Simulation Package)[61, 62, 63, 64]. All results reported have been obtained with projector-augmented-wave potentials using a 450 eV plane-wave cut-off [65, 66]. The Generalized Gradient Approximation (GGA) of Perdew–Burke–Ernzehof (PBE)

functional was used for the exchange-correlation term [67, 68]. We used a Methfessel–Paxton smearing [69]. Because of the large unit cell size used in calculations, the Brillouin-zone sampling was restricted to the Γ-point [70]. Van der Waals contributions were considered in the local van der Waals density functional scheme proposed by Dion et al [71] and Klimeŝ et al [72, 73, 74] and calculations were carried out using OptB86b-vdw level [73]. Atomic positions were relaxed with the conjugate gradient (CG) algorithm until forces on each moving atom were less than 0.02 eVÅ^{-1}.

In the unit cell, the substrate is represented by four layers of copper metal having the (111) orientation and covered by a (111)-oriented Cu_2O ultrathin oxide film with thickness of 5.89 or 11.07 Å. The detailed description (construction, optimisation, energetic and electronic properties and reactivity with water and OH groups) of the model will be presented in a separate article. Only a summary is given below. The MBT molecules were adsorbed on top of the oxide layer. The vacuum region was set at more than 18 Å to minimize the interactions in the z direction between periodic images of the system.

2.1. Passivated surface model

Fig.1 shows the constructed model of the passivated surface as derived from experimental data [75, 76, 77, 78, 79]. The model elaborated for the oxidized Cu(111)||Cu_2O(111) surface consists of the Cu(111) metal substrate covered by the stoichiometric Cu_2O(111) oxide film in parallel epitaxy: Cu(111)[110]||Cu_2O(111)[110]. Because of the perfect fit between the oxide and metal substrate lattices over a coincidence length of 17.87 Å[76, 79], we use the lateral dimensions of the supercell of 17.81 Å in both x and y directions, which corresponds to (7×7) and (6×6) supercells for Cu(111) and Cu_2O(111), respectively.

The two studied thicknesses of the oxide structure, 5.89 Å and 11.07 Å, correspond to two and four Cu_2O(111) layers, respectively. The oxide layers are kept free to move. The two bottom layers of the Cu(111) metal are fixed and two interface layers are kept free to move, aiming to optimize the interface interaction with the oxide film.

For the adsorption of the organic molecule, we considered three surface states of the oxide layer as shown in Fig.1. In the dry surface state, the bare Cu_2O(111) surface exhibits two distinct copper sites: coordinatively saturated (*csa*) and coordinatively unsaturated (*cus*) Cu atoms, labeled as Cu_{csa} and Cu_{cus}, respectively. It contains also two distinct oxygen sites:

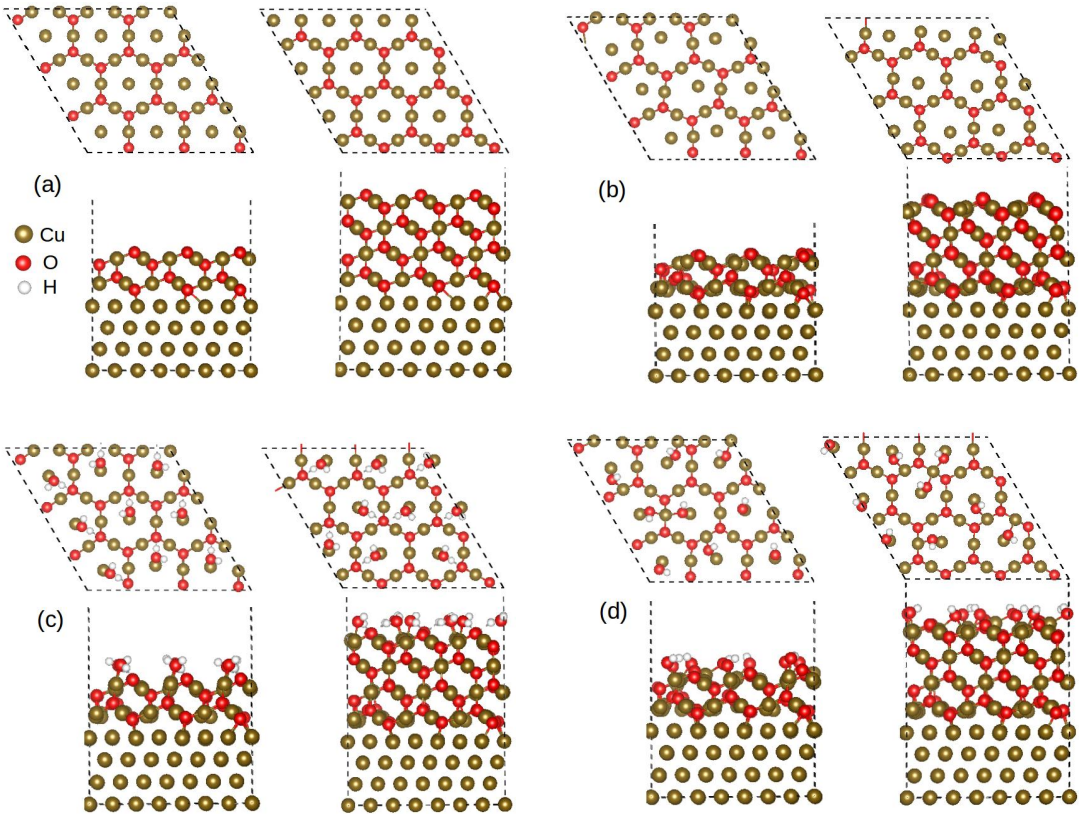

Figure 1: Snapshots of Cu(111) covered by two or four Cu_2O(111) oxide layers with different oxide surface states (top view and side view). Before relaxation (a) and after relaxation in the (b) dry, (c) hydrated and (d) hydroxylated surface states.

saturated and unsaturated oxygen ions, labeled (O_{dn}) and (O_{up}), respectively, where the subscripts indicate that they are located below (dn) and above (up) the surface Cu layer, as illustrated in Fig.2. The high symmetry of the unsaturated copper atoms is broken by lateral relaxation toward one or two adjacent saturated copper ions, which can affect the molecule adsorption topologies.

We also investigated the adsorption of the molecules on the hydrated and hydroxylated surfaces. Indeed, in contact with an aqueous solution, the surface can be covered by a layer of water molecules or by OH groups. On the hydrated surface, the water molecules bind on top of Cu_{cus} sites via the oxygen atom and form H-bonds with adjacent O_{up} oxygen. The adsorption energy is -1.10 eV/mol at saturation of the Cu_{cus} sites . On the

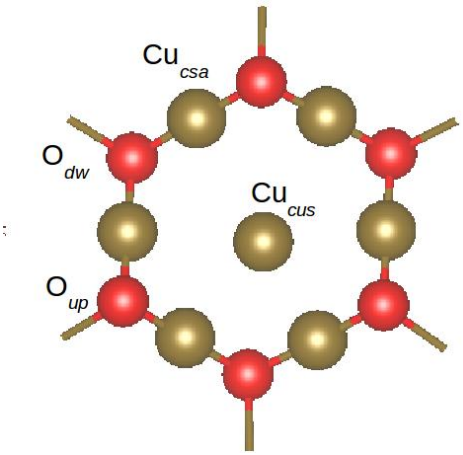

Figure 2: Surface sites of $Cu_2O(111)$. Cu_{cus} and Cu_{csa} correspond to unsaturated and saturated copper surface sites, respectively. O_{up} and O_{dn} correspond to unsaturated and saturated oxygen surface sites, respectively.

hydroxylated surface, two types of OH bonding, named μ_1-OH and μ_2-OH groups are found. μ_1-OH corresponds to OH adsorbed on top of Cu_{cus} atom, whereas μ_2-OH corresponds to OH adsorbed in bridge mode between Cu_{cus} and adjacent Cu_{csa} copper atoms. The adsorption energy at saturation is -3.72 eV/mol.

The supercell described here allows us to study MBT adsorption at low (0.37 mol/nm^2) and high coverage (3.27 mol/nm^2). The low coverage corresponds to one molecule per supercell and the high coverage to nine molecules per supercell, i.e. one molecule is adsorbed on each unsaturated copper site.

2.2. Molecules

The MBT molecule was modeled in thione (MBTH) and radical thiolate (MBT°) forms (Fig.3). The properties of the MBT molecule have been described in the literature. In the crystal structure, the molecules form centrosymmetric hydrogen bonded dimers [80, 81]. In dilute solution, MBT exists as thione monomer and cyclic dimer [82, 83]. Experimental [82, 44] and theoretical [54, 83] works revealed that the thione form is more stable than the thiol form, and thus the thiol form was not modeled in the present work. The isolated molecules were optimised in a box with dimensions of 20Å×20Å×20Å in x, y, and z directions, using the same computational conditions described above. For the radical MBT° form, spin polarization was implemented to get the energy minimum.

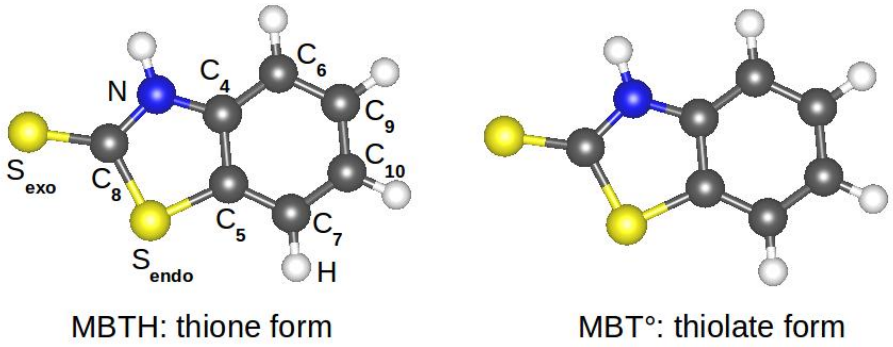

Figure 3: Isolated MBT molecule under the thione (MBTH) and thiolate (MBT°) forms modeled in this work

2.3. Energetics

The adsorption energy of the thione form (MBTH) was calculated as:

$$E_{ads} = [E(slab/MBTH) – E(slab) – nE(MBTH)]/n \quad (1)$$

where E(slab/MBTH) is the total energy of the system with MBTH adsorbed on the slab surface. E(slab) and E(MBTH) are the energies of the bare, relaxed Cu(111)||Cu_2O(111) slab and of the free MBTH molecule optimized in vacuum, respectively. n is the number of molecules on the surface.

The adsorption energy for the radical thiolate form (MBT°) was calculated as:

$$E_{ads} = [E(slab/MBT^{\circ}) – E(slab) – nE(MBT^{\circ})]/n \quad (2)$$

where E(slab/MBT°) is the total energy of the system with MBT° adsorbed on the slab surface. E(MBT°) is the energy of the free radical MBT° optimized in vacuum and n is the number of radical adsorbates on the surface.

In order to compare the stability of the formation of dense layer at full coverage with the adsorption at low coverage, we normalized the adsorption energy per unit area as follows:

$$\varepsilon_{norm} = E_{ads} \times \theta \quad (3)$$

where E_{ads} is the adsorption energy per molecule and $\theta = \frac{n}{A}$ is the coverage, defined as the number of adsorbed molecules (n) per area (A) of the slab.

We evaluated the interaction of MBTH and MBT° with the hydrated surface considering a substitution reaction, where MBT replaces H_2O on the surface covered initially by water molecules and water molecules are released after adsorption. The reaction is:

$$MBT + H_2O_{ads} \longrightarrow MBT_{ads} + H_2O \quad (4)$$

where H_2O_{ads} stands for adsorbed H_2O molecules and MBT_{ads} for adsorbed MBT molecules (MBTH or MBT° form). The corresponding substitution energy is calculated as:

$$\Delta E_{subst} = [E(slab/MBT) + nE(H_2O) - E(slab/H_2O) - nE(MBT)]/n \quad (5)$$

where E(slab/MBT) is the total energy of the system with MBT (MBTH or MBT°) adsorbed on the slab surface. E(H_2O) is the energy of a water molecule calculated in the vacuum. E(slab/H_2O) and E(MBT) are the energies of the optimized structures with the water molecules adsorbed on the surface and the free MBTH or MBT° form optimized in vacuum, respectively. n is the number of adsorbed (or released) molecules.

We also evaluated the interaction of the thione form (MBTH) with the hydroxylated surface. The following condensation reaction (replacement of an OH group by the MBT° form and release of water molecule) was considered:

$$MBTH + OH_{ads} \longrightarrow MBT_{ads} + H_2O \quad (6)$$

where OH_{ads} stands for a surface OH group and MBT_{ads} for an adsorbed molecule under thiolate form after reaction. The corresponding condensation energy is calculated as:

$$\Delta E_{cond.} = [E(slab/MBT^{\circ}) + nE(H_2O) - E(slab/OH) - nE(MBTH)]/n \quad (7)$$

where $E(slab/MBT^{\circ})$ is the total energy of the system with MBT thiolate (MBT°) adsorbed on the oxide surface. E(H_2O) is the energy of a water molecule calculated in the vacuum. E(slab/OH) and E(MBTH) are the energies of the optimized hydroxylated slab surface and the free MBTH thione form optimized in vacuum, respectively. n is the number of adsorbed MBT molecules.

2.4. Electronic and charge analysis

We plotted the charge density difference expressed as follows:

$$\Delta\rho(r) = \rho(r)_{slab/mol} - (\rho(r)_{slab} + \rho(r)_{mol}) \quad (8)$$

where $\rho(r)_{slab/mol}$ is the charge density distribution on the adsorbed system, $\rho(r)_{slab}$ and $\rho(r)_{mol}$ are the charge density distributions on the isolated slab and the molecule for the geometry after adsorption, respectively.
The net charge variation was determined on each atom by:

$$\Delta Q(x) = Q_{ads}(x) - Q_{vac}(x) \quad (9)$$

where $Q_{ads}(x)$ and $Q_{vac}(x)$ are the net charges on each atom (Bader population analysis) [84] of the adsorbed and free molecule, respectively.

3. Results and discussion

3.1. Adsorption topologies and energetics

The main question to answer is whether the molecules may adsorb on the oxidized surface and what are the most favored configurations obtained for a full MBT layer. The molecules were adsorbed on the dry, hydrated and hydroxylated surfaces.

A wide range of configurations were tested, considering: i) the different possible adsorption sites present on the topmost surface plane; ii) the different reactive sites of the molecule, which are the exo (S_{exo}) and endo (S_{endo}) cyclic sulfur, and the nitrogen atoms; iii) the orientation of the molecule with respect to the surface plane. We considered perpendicular, tilted and parallel orientations. Among all adsorption configurations investigated in this study, we discuss here the most relevant ones. An intuitive nomenclature is used to describe the adsorbed configurations. For example (S_{exo}-Cu_{cus}, NH-O_{up}) means that MBTH forms two bonds, one between the exocyclic sulfur (S_{exo}) atom and the unsaturated copper (Cu_{cus}) atom, the other one between the NH function and the oxygen atom located "up" (O_{up}) in the topmost oxide plane.

The energetics of MBTH and MBT° adsorption at low and high coverages is compiled in Table 1. As we did not find any difference for the adsorption mode of MBT on the models with two or four oxide layers, we discuss here in details only the case where Cu(111) is covered by two Cu_2O(111) oxide layers. The adsorption energy as function of the number of oxide layers is reported in each Figure.

	Low coverage (0.37 mol/nm^2)			Full coverage (3.27 mol/nm^2)				
	Fig.	E_{ads} (eV/mol)	ε_{norm} (J/m^2)	Fig.	E_{ads} (eV/mol)	ε_{norm} (J/m^2)	$\Delta E_{subst.}$ (eV/mol)	$\Delta E_{cond.}$ (eV/mol)
MBTH	Fig.4	-3.40	-0.20	Fig.5(a)	-2.71	-1.42	-1.61	-
MBT°	Fig.6	-4.60	-0.27	Fig.7(b)	-2.96	-1.55	-1.87	-1.35
				Fig.7(d)	-2.94	-1.54	-1.84	-1.33
				Fig.8(a)	-3.11	-1.63	-2.01	-1.50

Table 1: Energetics of MBT adsorption at low and full coverage on Cu(111) covered by two layers of Cu_2O(111). E_{ads} is the adsorption energy on the dry surface, calculated with Equations 1 and 2, ε_{norm} is the adsorption energy normalized per unit area, calculated with Equation 3. $\Delta E_{subst.}$ is the energy of substitution on the hydrated surface (Equation 5) and $\Delta E_{cond.}$ the energy of condensation on the hydroxylated surface (Equation 7).

3.1.1. Adsorption of thione form (MBTH) at low and full coverage

Fig.4 shows the most stable configuration obtained at low coverage. The molecule is tilted toward the surface (meaning rings nearly parallel to the surface). The adsorption energy is -3.40 eV/mol and ε_{norm} is -0.20 J/m^2. MBTH binds via the S_{exo} atom to a Cu_{cus} atom with a bond length of 2.17 Å. A NH....O hydrogen bond with an O_{up} atom is also formed and the distance NH...O is 1.61 Å. In addition, two carbon atoms of the aromatic ring are involved in the interaction mechanism. These carbon atoms (corresponding to C_6 and C_9 in Fig.3) are bonded to adjacent Cu_{cus} atoms with C-Cu bond lengths of 2.16 Å and 2.19 Å.

At high coverage, the molecules stand perpendicular to the surface in the most stable configuration (Fig.5(a)). The S_{exo} atom and the NH group are directed toward the surface. MBTH forms a covalent bond between the S_{exo} and a Cu_{cus} atoms with a bond length of 2.15 Å and an H-bond between the NH group and an unsaturated oxygen (O_{up}) surface atom (1.38 and 1.70 Å for NH...O). The adsorption direction from Cu_{cus} to O_{up} on the surface is favored over Cu_{cus} to O_{dn} by the formation of the H-bond (Fig.5 (a) and (b)). The adsorption energy is -2.71 eV/mol and less favorable than at low coverage. However, the normalization of the adsorption energy to a unit area, ε_{norm} = -1.42 J/m^2, shows that the formation of a full monolayer is much favored compared to the adsorption at low coverage. The adsorption of the molecule via both the exo and endocyclic sulfur atoms is less stable as shown in Fig.5 (c) and (d).

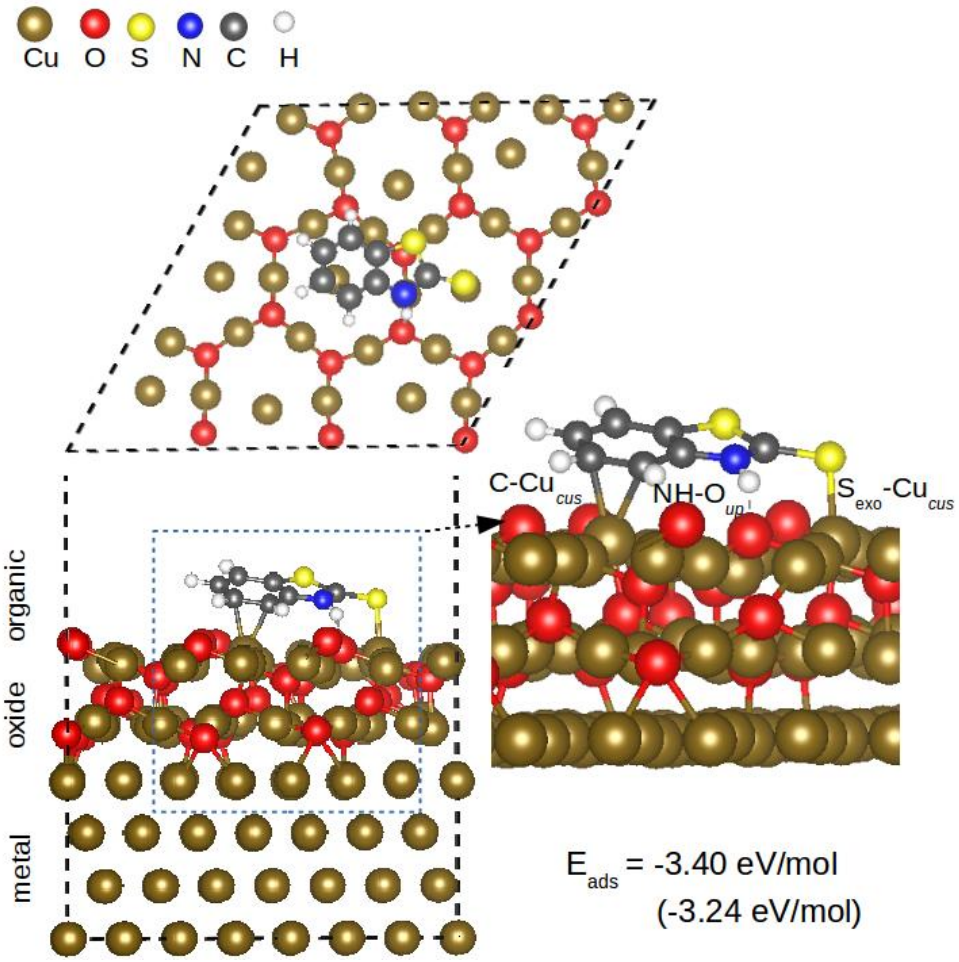

Figure 4: Snapshot and adsorption energy of the most stable adsorbed configuration of thione form (MBTH) at low coverage. E_{ads} value in brackets corresponds to the adsorption energy of MBTH adsorbed on Cu(111) covered by four Cu_2O(111) oxide layers.

3.1.2. Adsorption of thiolate form (MBT°) at low and full coverage

The situation for the thiolate is different since the molecule cannot form a H-bond with a surface oxygen. However, the nitrogen atom can interact directly with surface copper atoms. In addition, the reactivity of the molecule may be different in the radical form as compared to the neutral form.

The most stable adsorption configuration of MBT° at low coverage is a tilted orientation toward the surface (meaning rings nearly parallel to the surface), like for MBTH form (Fig.6(a)). Indeed, MBT° binds via the exo-

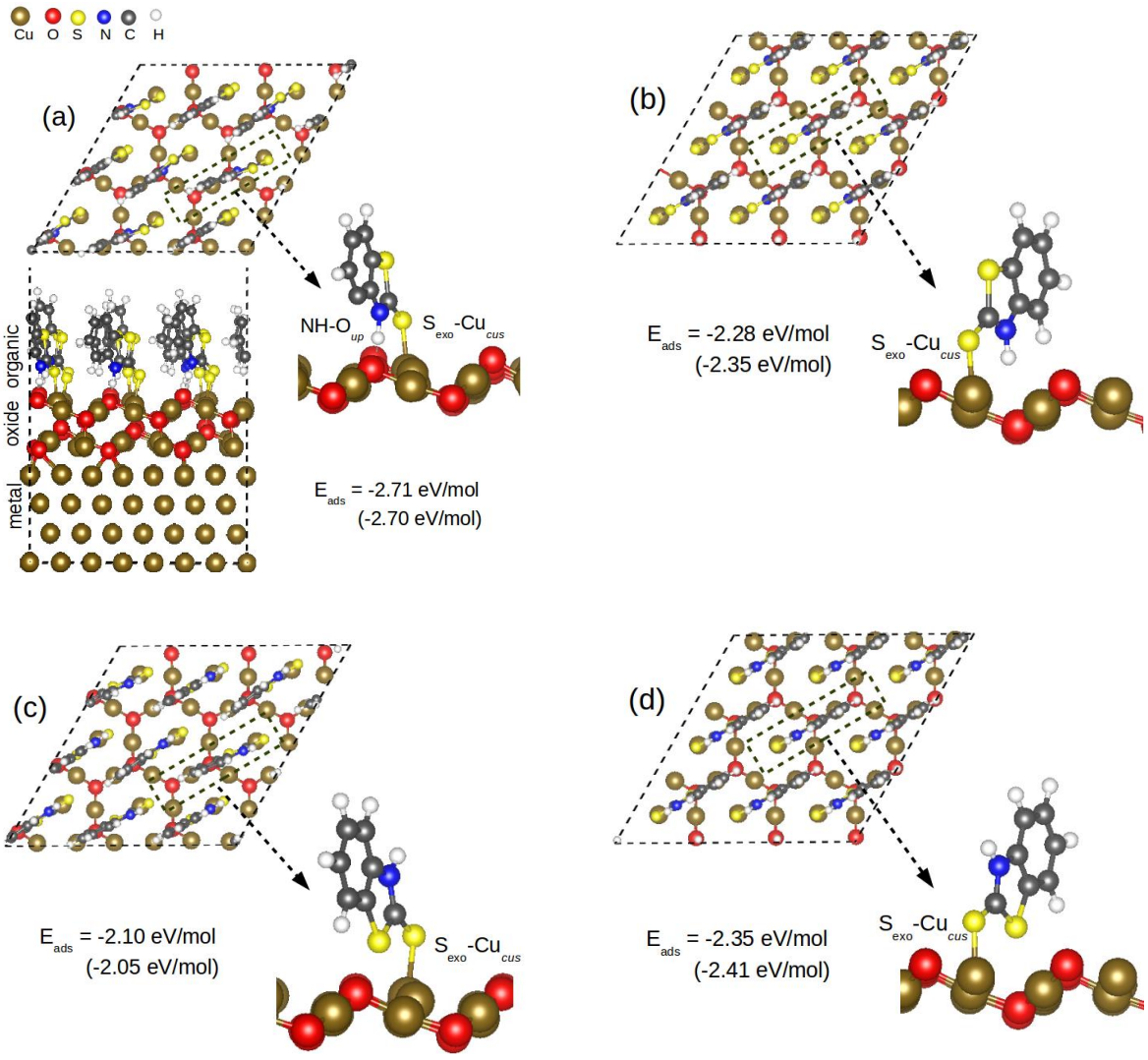

Figure 5: Snapshots and adsorption energies of different adsorption configurations of MBTH form at full coverage and illustration of the adsorption mode. Top, adsorption through exocyclic sulfur atom and NH functional group and orientation relative to the surface sites, (a): (S_{exo}-Cu_{cus} bond; NH-O_{up} bond) and (b): (S_{exo}-Cu_{cus} bond; NH-O_{dn} orientation). Bottom, adsorption through exo and endocyclic sulfur atoms and orientation relative to the surface sites, (c): (S_{exo}-Cu_{cus} bond; S_{endo}-O_{up} orientation) and (d): (S_{exo}-Cu_{cus} bond; S_{endo}-O_{dn} orientation). E_{ads} values in brackets correspond to the adsorption energy of MBTH adsorbed on Cu(111) covered by four Cu_2O(111) oxide layers.

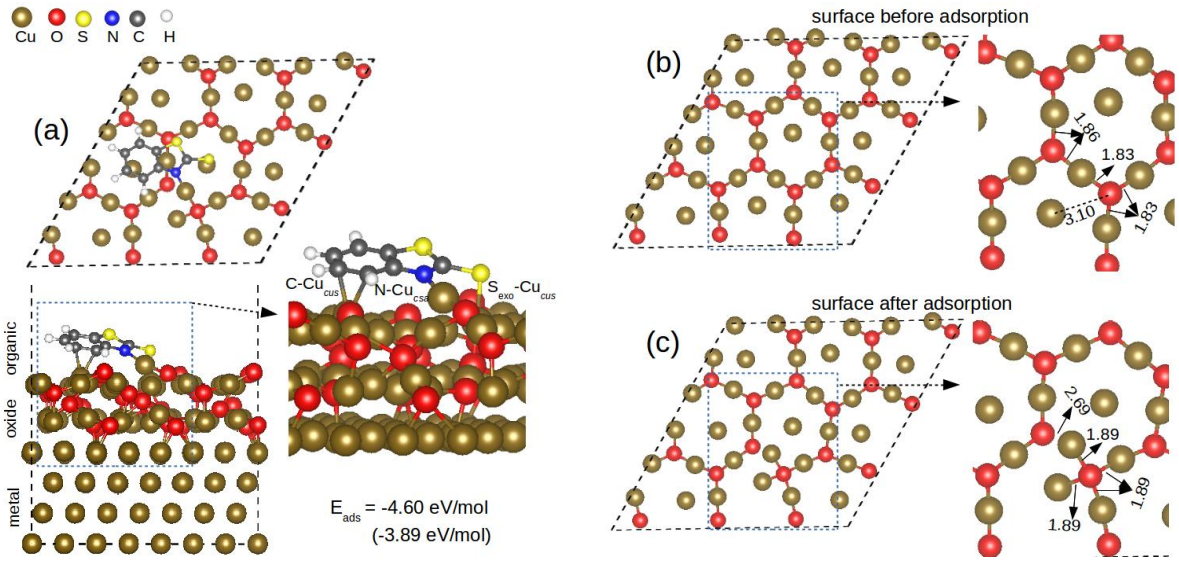

Figure 6: Snapshots and adsorption energy of the most stable adsorption configuration of thiolate form (MBT°) at low coverage (a) and surface structure of $Cu_2O(111)$ film after adsorption (b) and before adsorption (bare surface) (c). E_{ads} value in brackets corresponds to the adsorption energy of MBT° adsorbed on Cu(111) covered by four $Cu_2O(111)$ oxide layers.

cyclic sulfur to an unsaturated copper atom with a bond length of 2.18 Å. Two carbon atoms (C_6 and C_9 in Figure 3(b)) are also involved in the interaction mechanism with bond lengths C...Cu_{cus} of 2.11 Å and 2.14 Å. MBT° also forms a covalent bond via the nitrogen atom with a saturated copper atom with a bond length of 1.91 Å. The adsorption energy is -4.60 eV/mol (ε_{norm}= -0.27 J/m^2), which is more stable by 1.20 eV/mol than for MBTH. However, the competitive adsorption of both forms under the following mechanisms (MBTH + * $\longrightarrow$ MBT$_{ads}$ + $\frac{1}{2}$ H_2 or MBTH + * $\longrightarrow$ MBT$_{ads}$ + H_{ads}) showed that MBTH is more favored by 0.35 and 0.23 eV/mol, respectively. The results reveal that the competitive adsorption of MBT° is favored only in the presence of both species (thione and thiolate) in the same solution.

The surface atoms involved in the interaction undergo reconstruction (Fig.6(c)) as compared to the bare surface before adsorption (Fig.6(b)). Dehydrogenation of the molecule (MBT°) makes the nitrogen more reactive towards the substrate surface. The saturated copper atom is pulled out by breaking of the O_{dn}...Cu_{csa} bond due to the formation of the N...Cu_{csa} bond,

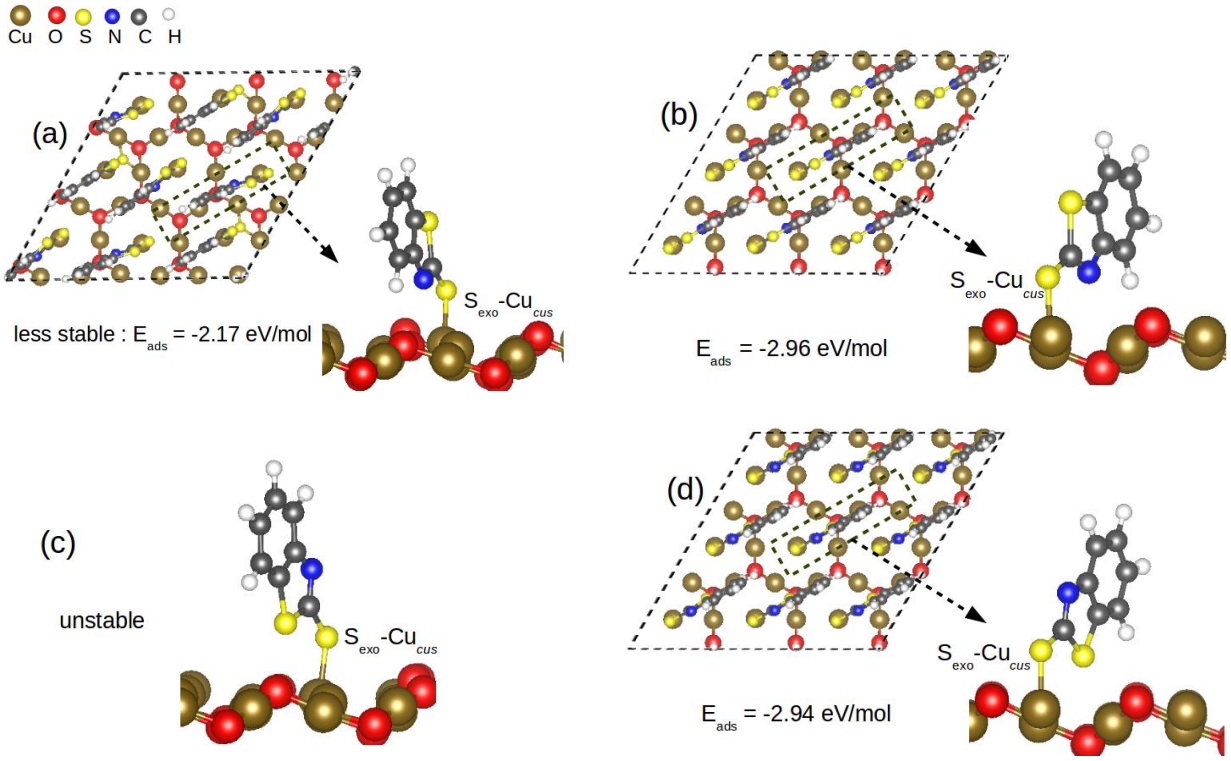

Figure 7: Snapshots and adsorption energies of different adsorption configurations of MBT° form at full coverage and illustration of different adsorption modes. Top, adsorption through exocyclic sulfur and nitrogen atoms and orientation relative to the surface sites, (a): (S_{exo}-Cu_{cus} bond; N-O_{up} orientation), (b): (S_{exo}-Cu_{cus} bond; N-O_{dn} orientation). Bottom, adsorption through exo and endocyclic sulfur atoms and orientation relative to the surface sites, (c): (S_{exo}-Cu_{cus} bond; S_{endo}-O_{up} orientation), (d): (S_{exo}-Cu_{cus} bond; S_{endo}-O_{dn} orientation).

and the O_{dn}...Cu_{csa} distance increases from 1.86 to 2.69 Å. Another change in the surface structure concerns the neighboring unsaturated copper atom, which moves and binds with the unsaturated oxygen (O_{up}) atom, the distance decreasing from 3.10 to 1.89 Å.

Different adsorption configurations studied at full coverage are shown in Fig.7 and Fig.8. In order to compare with the interaction of MBTH (Fig.5), we addressed similar adsorption configurations of MBT° bonded to Cu and O surface atoms as shown in Fig.7. The most stable configuration of MBT° is in Fig.8(a). The unstable (Fig.7(c) and Fig.8(b)) and less stable (Fig.7(a))

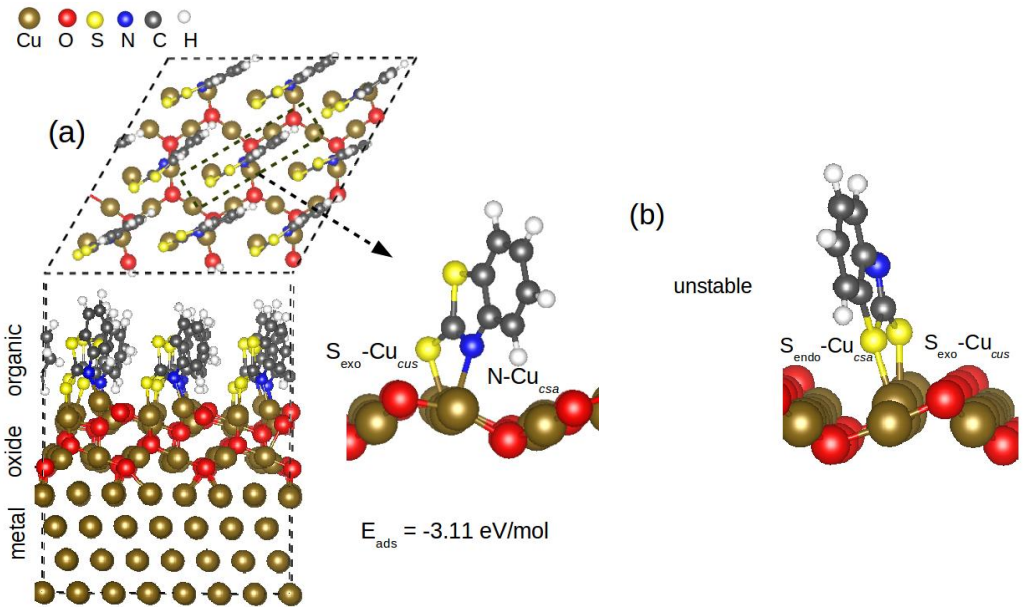

Figure 8: Snapshots and adsorption energy of different adsorption configurations of MBT° at full coverage and illustration of different adsorption modes. (a) adsorption through exocyclic sulfur and nitrogen atoms and orientation relative to the surface sites (S_{exo}-Cu_{cus} bond; N-Cu_{csa} bond). (b) adsorption through exo and endocyclic sulfur atoms and orientation relative to the surface sites (S_{exo}-Cu_{cus} bond; S_{endo}-Cu_{csa} bond).

configurations are not further discussed below.

At full coverage, MBT°, like MBTH, adsorbs in a perpendicular orientation. Interestingly, the adsorption via S_{exo} and N atoms or via S_{exo} and S_{endo} atoms, noted (b) and (d) in Fig.7, respectively, are iso-energetic. The adsorption energy is -2.95±0.01 eV/mol (ε_{norm}= -1.55 J/m^2) and more stable by 0.25 eV/mol than for MBTH. This competitive adsorption is valid only in the presence of both species (thione and thiolate) in the same medium, as explained for low coverage case. MBT° binds only via S_{exo} atom to an unsaturated copper atom, with a bond length of 2.12 Å. The distance from the S_{endo} and N atoms to the O_{dn} atom is 3.15±0.03 and 4.48±0.03 Å, respectively. These MBT° adsorbed configurations are oriented from Cu_{cus} to O_{dn} direction, whereas it is from Cu_{cus} to O_{up} direction for the most stable configuration of MBTH.

The most stable adsorbed configuration of MBT°, noted (a) in Fig.8, has an adsorption energy of -3.11 eV/mol (ε_{norm} = -1.63 J/m^2). The normalization to the unit area shows again that the full monolayer adsorption is favored

compared to the low coverage adsorption. MBT° binds via S_{exo} atom to an unsaturated copper atom, with a bond length of 2.12 Å. In addition, MBT° forms a covalent bond via its nitrogen atom with a saturated copper surface, with a bond length of 1.98±0.04 Å.

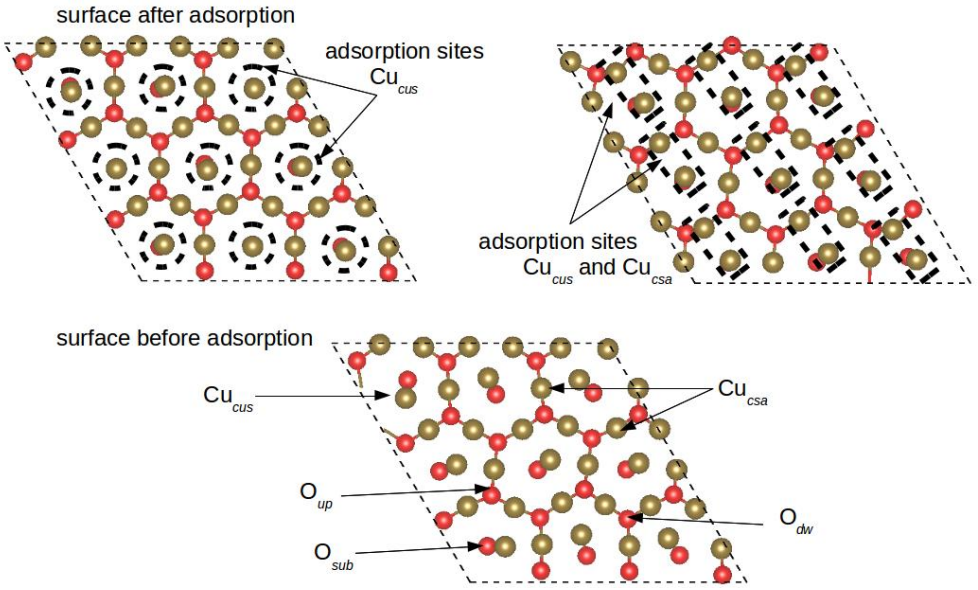

Figure 9: Surface structure after adsorption of MBT (top) compared to bare surface structure (bottom). Top left corresponds to all adsorption configurations of MBTH and MBT° with one covalent bond of the molecule to the Cu_{cus} atom (circled). Top right corresponds to the configuration in Fig8(a) with two covalent bonds of the molecule to the Cu_{cus} and Cu_{csa} atoms (circled).

We recall that on bare $Cu_2O(111)$ surface the high-symmetry of the Cu_{cus} atom is broken due to lateral relaxation towards adjacent Cu_{csa} ions. At full coverage, the adsorption of the molecule under MBTH and MBT° forms on top of the Cu_{cus} atoms lifts the reconstruction of the bare surface (Fig.9) and the bulk high-symmetry is recovered. Thus both forms of molecule stabilize the Cu_{cus} sites. However, for the most stable adsorbed configuration of MBT° shown in Fig.8(a), the Cu_{csa} atoms are also involved in the interaction mechanism. The nitrogen atom pulls out the Cu_{csa} atom with elongation of the O-Cu_{csa} distance (average of Δd = 0.12 Å), indicating a quasi-bond breaking (Cu_{csa}...O_{dn} or Cu_{csa}...O_{up}) compensated by bond-making between Cu and N atoms (Cu_{csa}...N).

Comparison of the adsorption energies (E_{ads}) calculated by Equations 1 and 2, and substitution energy (E_{subs}) calculated by Equation 5, from the mechanism defined by Equation 4, shows that the formation of an MBTH or MBT° adsorbed monolayer at full coverage is much more exothermic than that of a molecular water layer (Table 1). Indeed, we calculated substitution energies of -1.61 and -2.01 eV/mol for the most stable monolayer configuration of MBTH (Fig.5 (a)) and MBT° (Fig.8 (a)), respectively. This means that in both forms the MBT molecule is able to substitute a water monolayer on the hydrated copper oxide surface. However, the substitution mechanism of hydroxyl groups, OH_{ads} + MBT $\longrightarrow$ MBT_{ads} + OH , is unfavored for both the MBTH and MBT° forms. For these reasons, we considered the condensation reaction of MBT° (Equation 6) with the corresponding energy calculated by Equation 7. The results show that this condensation reaction is very exothermic with calculated energies of -1.34±0.01 eV/mol for (b) and (d) configurations in Fig.7 and -1.50 eV/mol for (a) configuration in Fig.8. These calculations suggest that the MBTH form would be able to replace surface OH groups by forming adsorbed MBT° and releasing water but that the MBT° form would not be able to directly substitute surface OH groups.

We can conclude that whatever the surface state of the $Cu_2O(111)$ oxide film on Cu(111) (anhydrous, hydrated or hydroxylated) the adsorption of MBT (under thione and thiolate forms) is favored and MBT can form dense and ordered monolayer with a density of 3.27 mol/nm^2, which could explain the experimental results on the formation of the protective film on copper under different conditions [15, 16]. However, the adsorption mode depends on the thione or thiolate form of the MBT molecule and the copper surface state (covered or not by oxide). The thione form (MBTH) is adsorbed via covalent bonding of the S_{exo} atom on $Cu(111)||Cu_2O(111)$ surfaces, which corresponds to the bonding reported from experimental measurement on oxidized copper by Woods et al. [21]. The thiolate form (MBT°) is adsorbed via covalent bonding of both the N and S_{exo} atoms on $Cu(111)||Cu_2O(111)$ surfaces, in agreement with the bonding reported from XPS measurements by Kazansky et al. [20] and Finšgar and Merl [19]. On the metallic surface not covered by any oxide, the adsorption via covalent bonding of both exo and endocyclic S atoms was calculated to take place on metallic copper [54] and observed experimentally by XPS [26, 27]. This type of bonding was also observed on metallic gold by STM measurements [49].

3.2. Electronic structure analysis

Electronic structure analysis provides more details about the molecule-surface interaction. This can be done using the density of states (DOS), the projected density of states (PDOS), the integral local density of states (ILDOS) and the visualization of the molecular orbitals. It can be also done by analysis of the charge density variation ($\Delta\rho(r)$) and charge transfer (Δ Q) as defined in Equations 8 and 9, respectively. A combined analysis of all these data brings relevant information useful to understand the nature of the reactive sites involved in the binding process, the amount of charge transferred from/to the surface, and the reactivity of the molecules towards substrate surfaces.

3.2.1. Isolated species (before adsorption)

The total density of state (DOS) analysis of the isolated thione (MBTH) form is shown in Fig.10 (middle). There are several S, N, C and H atoms in the molecule, and hence, we projected the density of states (PDOS) for every type of atom, as shown in Fig.10 (bottom). The molecular orbitals of the isolated molecules and the integral range are shown in Fig.10 (top). We represented the highest occupied molecular orbitals (HOMO-1 and HOMO) and lowest unoccupied molecular orbitals LUMO and LUMO+1, with iso-surface of +0.004 e/Å^3.

The DOS shows that the HOMO is located near the Fermi level of the slab at about -0.40 eV and that the LUMO is located 2.70 eV above the Fermi level. These HOMO and LUMO alignments relative to the Fermi level suggests that MBTH can easily exchange electrons with the surface and behaves more as an electron donor than electron acceptor during the adsorption process. The PDOS reveals that the occupied states near the Fermi level are dominated by the contribution of the exocyclic sulfur orbitals (green line). Thus, the exocyclic sulfur atom is the most reactive species and it is the most likely site for the interaction with the surface copper atoms. We also observe a small contribution of nitrogen and endocyclic sulfur atoms to the DOS, which is visible at HOMO and HOMO-1 levels. The LUMO and LUMO+1 levels show the contribution of all atomic orbitals of the molecule in the unoccupied states. Analysis for the isolated thiolate anion shows similar characteristics.

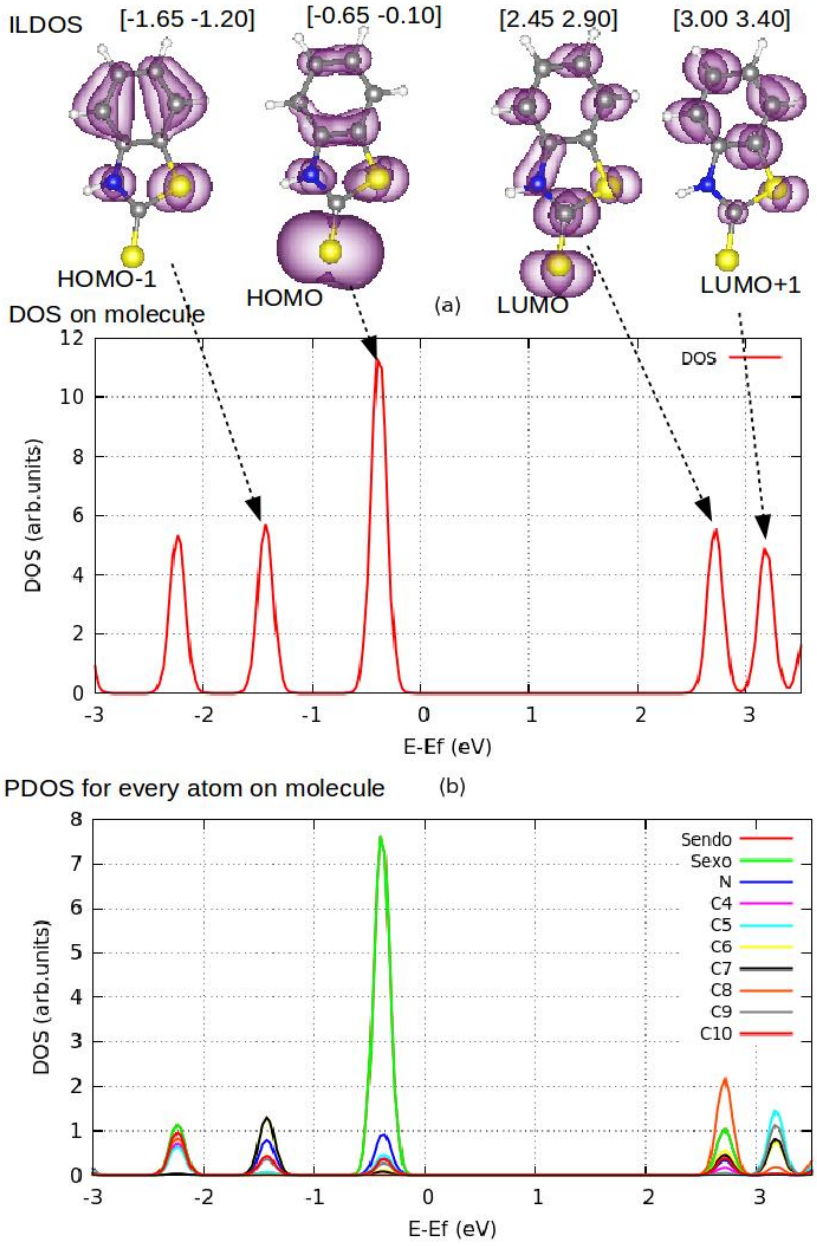

Figure 10: Electronic structure analysis of the isolated MBTH form of MBT: integral local density of states (ILDOS, top), density of states (DOS, middle) and projected density of states (PDOS, bottom).

3.2.2. Adsorbed molecules at full coverage

Fig.11 depicts the ILDOS (top) at different integral range, the PDOS on the molecule (middle) and for every atom (bottom) for MBTH adsorbed at full coverage. It corresponds to the most stable adsorbed configurations in Fig.5(a).

The comparison of the ILDOS and DOS projected on the molecules before and after adsorption, reveals drastic changes in the electronic structure of the molecule, indicating a strong molecule-surface interaction. We observe peak shifting, peak broadening, and the appearance of new peaks in the density of states after adsorption. Two peaks located below the Fermi energy at -1.50 eV and -3.60 eV are dominated by the DOS of the exocyclic sulfur atom. The ILDOS reveals that the peak at -1.50 eV is similar to the sulfur contribution at HOMO before adsorption and that the peak at lower energy (-3.60 eV) is associated to the sulfur-copper binding. It can be concluded that the interaction via the exocyclic sulfur with the copper atom is very strong and it is the only atom involved in the covalent binding of MBTH on $Cu(111)||Cu_2O(111)$ surface.

More details on the molecule-surface binding are provided by the charge density difference analysis. Fig.12 show the charge density difference ($\Delta\rho(r)$), plotted with an isosurface of ± 0.001 e/Å^3 for the most stable configuration at full coverage of MBTH. For better visualization of the isosurface, we represented only one molecule on the surface in the same adsorption topology as at full coverage.

$\Delta\rho(r)$ shows charge density accumulation between the exocyclic sulfur atom and one unsaturated copper. In addition a charge density deficit is observed on the S_{exo} and Cu_{cus} atoms, confirming again the formation of a covalent bond between these atoms. We also observe charge density accumulation on one unsaturated oxygen atom and charge density deficit on the hydrogen of the NH group confirming the H-bonding NH...O.

The Bader charge analysis for MBTH form reveals an electron transfer from the organic layer to the oxide. We calculated the values of 0.15 e/molecule at full coverage. The electrons were redistributed in the oxide, whereas the electrons distribution after adsorption remains unchanged in the metallic part of the slab substrate. The electrons redistribution on the

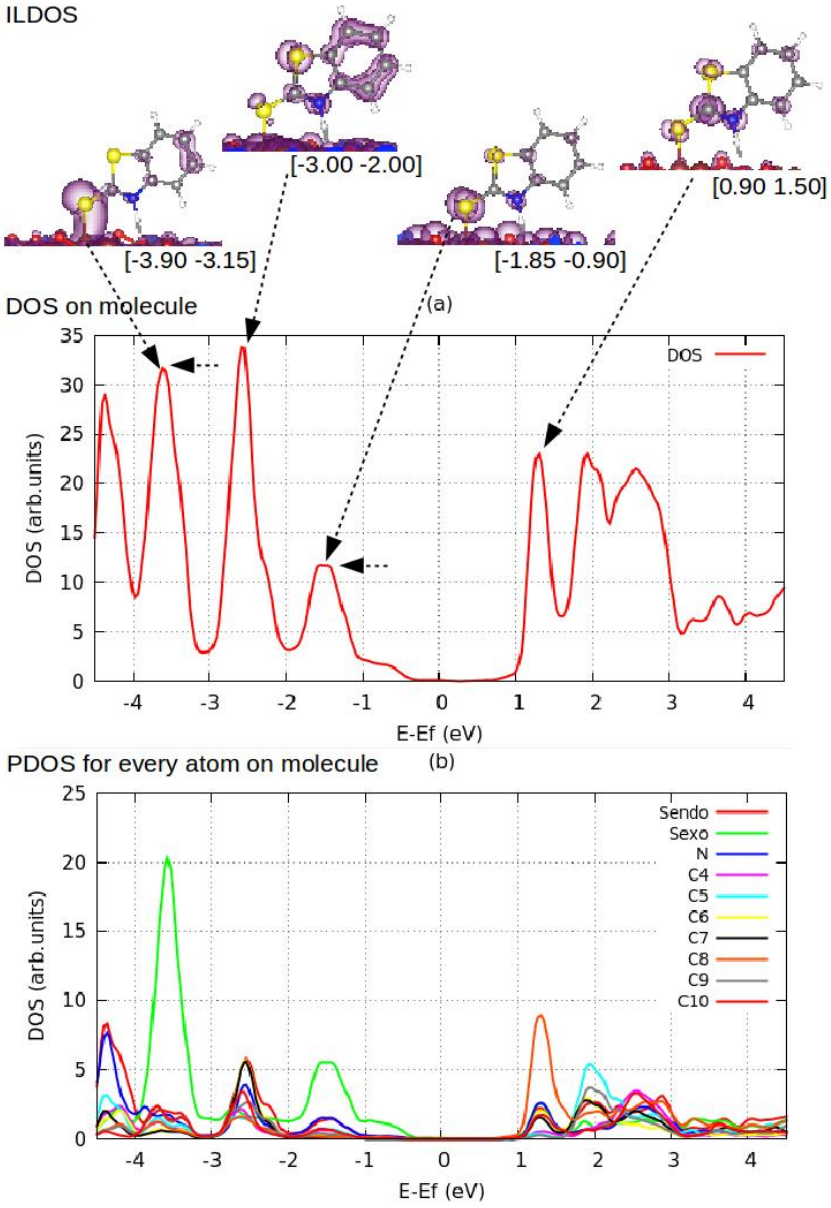

Figure 11: Electronic properties of adsorbed MBTH at full coverage: visualisation of integral local density of states (ILDOS, top), projected density of states on the molecules (PDOS, middle) and projected density of states for every atom of the molecule (PDOS, bottom).

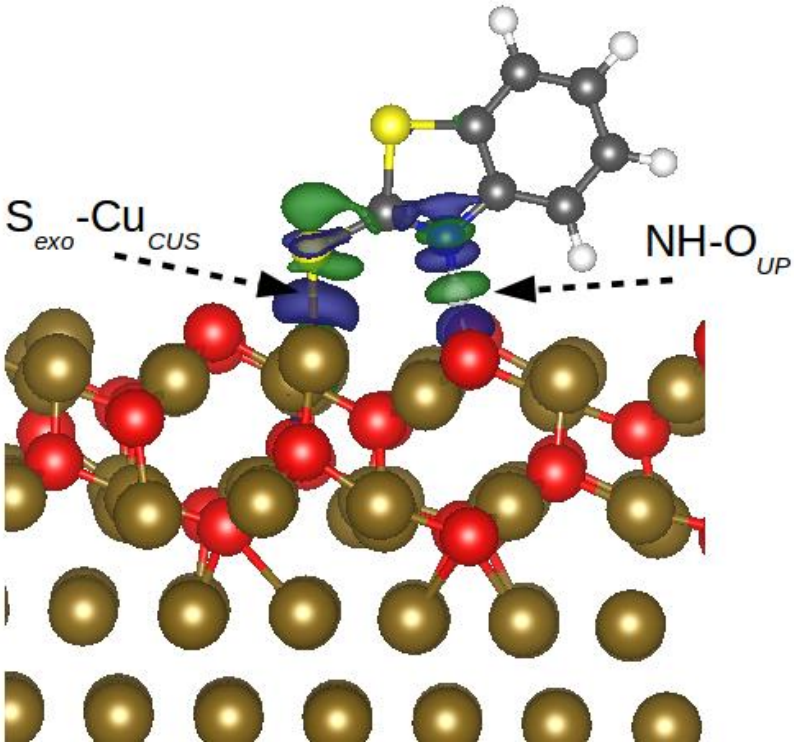

Figure 12: Charge density difference analysis for most stable full coverage adsorbed configuration of MBTH. Blue and green color correspond to accumulation and deficit of charge density, respectively

molecules concerns all atoms. The exocyclic sulfur atoms lose electrons, whereas endocyclic sulfur atoms gain electrons and the nitrogen atom charge remains unchanged before and after adsorption. Analysis for the most stable form of adsorbed thiolate at full coverage also confirms the nature of covalent bonding between the S_{exo} and Cu_{cus} atoms and between the N and Cu_{csa} atoms.

4. Conclusion

The interaction of the organic inhibitor 2-mercaptobenzothiole (MBT) under thione (MBTH) and thiolate (MBT°) forms with an oxidized copper surface modeled by a Cu(111)||Cu_2O(111) slab was investigated by DFT. We analyzed the structural and energetic trends to determine the most sta-

ble adsorption configuration, and more details about the molecule-surface interaction were provided by the electronic structure analysis.

Two thicknesses of the oxide overlayer were considered (5.89 and 11.07 Å) and gave similar results. The oxide surface was considered in the dry, hydrated and hydroxylated states at full coverage.

At low coverage, the molecules are in tilted adsorption mode. Both forms of MBT bind via S_{exo} atom to Cu_{cus} and two carbon atoms in the aromatic ring are bonded with adjacent Cu_{cus}. In addition MBT° binds via N atoms to Cu_{csa}, instead of NH...O_{up} H-bonding for MBTH.

At full coverage, the molecules can form a dense and ordered monolayer by standing perpendicular to the surface. The S_{exo}-Cu_{cus}; NH–O_{up} and S_{exo}-Cu_{cus}; N-Cu_{csa} orientations are favored for MBTH and MBT° forms, respectively. For both forms, the exocyclic sulfur atom is more reactive and binds covalently to Cu_{cus}. In the thiolate form, the nitrogen is more reactive and binds covalently to Cu_{csa}, whereas in the thione form, a NH...O_{up} H-bond is formed.

The adsorption of the molecules leads to recover the high symmetry of the Cu_{cus} sites broken on the bare $Cu_2O(111)$ surface. Thus both forms of the molecule are able to stabilize the surface by bond-making between the S_{exo} and Cu_{cus} atoms. However, for MBT°, bond making between the N and Cu_{csa} atoms leads to the surface reconstruction of Cu_{csa} sites by bond elongation with the adjacent O atoms.

The adsorption energy shows strong interaction of MBT with the $Cu(111)||Cu_2O(111)$ surface and a similar trend for the two studied Cu_2O layer thicknesses.

The normalization of the adsorption energy to a unit area shows that the full layer formation is favored as compared to the single molecule adsorption. The high adsorption energy is confirmed by the electronic analysis, which evidences the formation of strong bonds between the molecule and the oxidized copper surface. Our calculations suggest that the substitution of water or OH groups by MBT molecule is exothermic, the adsorption of MBT is favored whatever the surface state of the oxide film. All these results suggest that MBT strongly adsorbs on copper covered by an ultra thin oxide film and contribute to explain the corrosion protection efficiency of MBT molecule.

Acknowledgments

This project has received funding from the European Research Council (ERC) under the European Union's Horizon 2020 research and innovation

program (ERC Advanced Grant No. 741123, Corrosion Initiation Mechanisms at the Nanometric and Atomic Scales : CIMNAS).

References

[1] I. Milošev, Contemporary modes of corrosion protection and functionalization of materials, Acta Chim. Slov. 66 (2019) 511–533.

[2] S. Gangopadhyay, P. A. Mahanwar, Recent developments in the volatile corrosion inhibitor (VCI) coatings for metal: A review, J. Coat. Technol. Res. 15 (2018) 789–807.

[3] P. B. Raja, M. G. Sethuraman, Natural products as corrosion inhibitor for metals in corrosive media - A review,, Mater. Lett. 62 (2008) 113–116.

[4] R. L. Twite, G. P. Bierwagen, Review of alternatives to chromate for corrosion protection of aluminum aerospace alloys, Prog. Org. Coat. 33 (1998) 91–100.

[5] M. Kendig, S. Jeanjaquet, R. Addison, J. Waldrop, Role of hexavalent chromium in the inhibition of corrosion of aluminum alloys, Surf. and Coat. Techn. 140 (2001) 58–66.

[6] J. Sinko, Challenges of chromate inhibitor pigments replacement in organic coatings, Prog. Org. Coat. 42 (2001) 267–282.

[7] Y. Qiang, S. Zhang, S. Yan, X. Zou, S. Chen, Three indazole derivatives as corrosion inhibitors of copper in a neutral chloride solution, Corros. Sci. 126 (2017) 295–304.

[8] J. Li, C. W. Du, Z. Y. Liu, X. G. Li, M. Liu, Inhibition film formed by 2-mercaptobenzothiazole on copper surface and its degradation mechanism in sodium chloride solution, Int. J. Electrochem. Sci. 11 (2016) 10690–10705.

[9] Z. Tao, W. He, S. Wang, G. Zhou, Electrochemical study of cyproconazole as a novel corrosion inhibitor for copper in acidic solution, Ind. Eng. Chem. Res. 52 (2013) 17891–17899.

[10] H. Tian, W. Li, K. Cao, B. Hou, Potent inhibition of copper corrosion in neutral chloride media by novel non-toxic thiadiazole derivatives, Corros. Sci. 73 (2013) 281–291.

[11] M. Finšgar, 2-mercaptobenzimidazole as a copper corrosion inhibitor: Part II. surface analysis using X-ray photoelectron spectroscopy, Corros. Sci. 72 (2013) 90–98.

[12] Y. S. Tan, M. P. Srinivasan, S. O. Pehkonen, S. Y. M. Chooi, Effects of ring substituents on the protective properties of self-assembled benzenethiols on copper, Corros. Sci. 48 (2006) 840–862.

[13] R. Subramanian, V. Lakshminarayanan, Effect of adsorption of some azoles on copper passivation in alkaline, Corros. Sci. 44 (2002) 535–554.

[14] J. D. G. Xue, X. Y. Huang, J. Zhang, The formation of an effective anti-corrosion film on copper surfaces from 2-mercaptobenzimidazole solution, J. Electroanal. Chem. Interfacial Electrochem. 310 (1991) 139–148.

[15] D. Chadwick, T. Hashemi, Electron spectroscopy of corrosion inhibitors: Surface films formed by 2-mercaptobenzothiazole and 2-mercaptobenzimidazole on copper, Surf. Sci. 89 (1979) 649–659.

[16] M. Ohsawa, W. Suetaka, Spectro-electrochemical studies of the corrosion inhibittion of copper by 2-mercaptobenzothiazole, Corros. Sci. 19 (1979) 709–722.

[17] J. C. Marconato, L. O. Bulho, A spectroelectrochemical study of the inhibition of the electrode process on copper by 2- mercaptobenzothiazole in ethanolic solutions, Electrochim. Acta 43 (1998) 771–780.

[18] J. A. Ramírez-Cano, L. Veleva, R. M. Souto, B. M. Fernández-Pérez, SECM study of the pH distribution over Cu samples treated with 2-mercaptobenzothiazole in NaCl solution, Electrochem. commun. 78 (2017) 60–63.

[19] M. Finšgar, D. K. Merl, An electrochemical, long-term immersion, and XPS study of 2-mercaptobenzothiazole as a copper corrosion inhibitor in chloride solution, Corros. Sci. 83 (2014) 164–175.

[20] L. P. Kazansky, I. A. Selyaninov, Y. I. Kuznetsov, Adsorption of 2-mercaptobenzothiazole on copper surface from phosphate solutions, Appl. Surf. Sci. 258 (2012) 6807–6813.

[21] R. Woods, G. A. Hope, K. Watling, A SERS spectroelectrochemical investigation of the interaction of 2-mercaptobenzothiazole with copper, silver and gold surfaces, J. Appl. Electrochem. 30 (2000) 1209–1222.

[22] T. Shahrabi, H. Tavakholi, M. G. Hosseini, Corrosion inhibition of copper in sulphuric acid by some nitrogen heterocyclic compounds, Anti-Corrosion Methods and Materials 54 (2007) 308–313.

[23] D. He, F. Chen, J. Chen, S. Yao, W. Wei, Real-time bulk acoustic wave studies of the inhibition behavior of mercaptobenzothiazole on copper, Thin Solid Films 352 (1999) 234–238.

[24] Q. Bao, D. Zhang, Y. Wan, 2-mercaptobenzothiazole doped chitosan/11-alkanethiolate acid composite coating: Dual function for copper protection, Appl. Surf. Sci. 257 (2011) 10529–10534.

[25] Y.-H. Chen, A. Erbe, The multiple roles of an organic corrosion inhibitor on copper investigated by a combination of electrochemistry-coupled optical in situ spectroscopies, Corros. Sci. 145 (2018) 232–238.

[26] X. Wu, F. Wiame, V. Maurice, P. Marcus, Adsorption and thermal stability of 2-mercaptobenzothiazole corrosion inhibitor on metallic and pre-oxidized Cu(111) model surfaces, Applied Surface Science 508 (2020) 145132.

[27] X. Wu, F. Wiame, V. Maurice, P. Marcus, 2-mercaptobenzothiazole corrosion inhibitor deposited at ultra-low pressure on model copper surfaces, Corrosion science (2020). URL: https://doi.org/10.1016/j.corsci.2020.108464.

[28] P. J. Denissen, S. J. Garcia, Reducing subjectivity in EIS interpretation of corrosion and corrosion inhibition processes by in-situ optical analysis, Electrochim. Acta 293 (2019) 514–524.

[29] K. Xhanari, M. Finšgar, The corrosion inhibition of AA6082 aluminium alloy by certain azoles in chloride solution: Electrochemistry and surface analysis, Coating 9 (2019) 380.

[30] M. A. Zadeh, J. Tedim, M. Zheludkevich, S. van der Zwaag, S. J. Garcia, Synergetic active corrosion protection of AA2024-T3 by 2D- anionic and 3D-cationic nanocontainers loaded with Ce and mercaptobenzothiazole, Corros. Sci. 135 (2018) 35–45.

[31] P. Visser, H. Terryn, J. M. C. Mol, On the importance of irreversibility of corrosion inhibitors for active coating protection of AA2024-T3, Corros. Sci. 140 (2018) 272–285.

[32] A. C. Balaskas, T. Hashimoto, M. Curioni, G. E. Thompson, Two-shell structured PMAA@CeO_2 nanocontainers loaded with 2-mercaptobenzothiazole for corrosion protection of damaged epoxy coated AA2024-T3, Nanoscale 9 (2017) 5499.

[33] F. Maia, K. A. Yasakau, J. Carneiro, S. Kallip, J. Tedim, T. Henriques, A. Cabral, J. Venâncio, M. L. Zheludkevich, M. G. S. Ferreira, Corrosion protection of AA2024 by sol–gel coatings modified with MBT-loaded polyurea microcapsules, Chem. Eng. J. 283 (2016) 1108–1117.

[34] E. Roussi, A. Tsetsekou, A. Skarmoutsou, C. A. Charitidis, A. Karantonis, Anticorrosion and nanomechanical performance of hybrid organosilicate coatings integrating corrosion inhibitors, Surf. Coat. Techn. 232 (2013) 131–141.

[35] H. Cen, J. Cao, Z. Chen, X. Guo, 2-mercaptobenzothiazole as a corrosion inhibitor for carbon steel in supercritical CO_2-H_2O condition, Appl. Surf. Sci. 476 (2019) 422–434.

[36] Z. Mirzakhanzadeh, A. Kosari, M. H. Moayed, R. Naderi, P. Taheri, J. M. C. Mol, Enhanced corrosion protection of mild steel by the synergetic effect of zinc aluminum polyphosphate and 2-mercaptobenzimidazole inhibitors incorporated in epoxy-polyamide coatings, Corros. Sci. 138 (2018) 372–379.

[37] I. A. Kartsonakis, S. G. Stanciu, A. A. Matei, R. Hristu, A. Karantonis, C. A. Charitidis, A comparative study of corrosion inhibitors on hot-dip galvanized steel, Corros. Sci. 112 (2016) 289–307.

[38] K. Rahmani, R. Jadidian, S. Haghtalab, Evaluation of inhibitors and biocides on the corrosion, scaling and biofouling control of carbon steel

and copper–nickel alloys in a power plant cooling water system, Desalination 393 (2016) 174–185.

[39] M. Gholami, I. Danaee, M. H. Maddahy, M. RashvandAvei, Correlated ab initio and electroanalytical study on inhibition behavior of 2-mercaptobenzothiazole and its thiole thione tautomerism effect for the corrosion of steel (API 5L X52) in sulphuric acid solution, Ind. Eng. Chem. Res. 52 (2013) 14875–14889.

[40] J. Zhang, Q. Zhang, H. Ren, W. Zhao, H. Zhang, Inhibition performance of 2-mercaptobenzothiazole derivatives in CO_2 saturated solution and its adsorption behavior at Fe surface, Appl. Surf. Sci. 253 (2017) 7416–7422.

[41] L. P. Kazansky, Y. E. Pronin, I. A. Arkhipushkin, XPS study of adsorption of 2-mercaptobenzothiazole on a brass surface, Corros. Sci. 89 (2014) 21–29.

[42] K. Ramji, D. R. Cairns, S. Rajeswari, Synergistic inhibition effect of 2-mercaptobenzothiazole and Tween-80 on the corrosion of brass in NaCl solution, Appl. Surf. Sci. 254 (2008) 4483–4493.

[43] X. Xing, X. Xu, J. Wang, W. Hu, Preparation, release and anticorrosion behavior of a multi-corrosion inhibitors-halloysite nanocomposite, Chem. Phys. Lett. 718 (2019) 69–73.

[44] Y. Li, S. Zhang, Q. Ding, D. Feng, B. Qin, L. Hu, The corrosion and lubrication properties of 2-mercaptobenzothiazole functionalized ionic liquids for bronze, Tribology International 114 (2017) 121–131.

[45] D. Liu, E. Han, Y. Song, D. Shan, Enhancing the self-healing property by adding the synergetic corrosion inhibitors of Na_3PO_4 and 2-mercaptobenzothiazole into the coating of Mg alloy, Electrochim. Acta 323 (2019) 134796.

[46] Z.-H. Xie, S. Shan, Nanocontainers-enhanced self-healing Ni coating for corrosion protection of Mg alloy, J. Mater. Sci. 53 (2018) 3744–3755.

[47] H. Yang, Y. Sun, J. Ji, W. Song, X. Zhu, Y. Yao, Z. Zhang, 2-mercaptobenzothiazole monolayers on zinc and silver surfaces for anticorrosion, Corros. Sci. 50 (2008) 3160–3167.

[48] V. Grekulović, M. R. Vujasinović, A. Mitovski, Electrochemical behavior of AgCu50 in alkaline media in the presence of clorides and 2-mercaptobenzothiazole, J. Min. Metall. Sect. B-Metall 53 (2017) 349–356.

[49] B. Cui, T. Chen, D. Wang, L.-J. Wan, In situ STM evidence for the adsorption geometry of threen-heteroaromatic thiols on Au(111), Langmuir 27 (2011) 7614–7619.

[50] R. K. Shervedani, M. K. Babadi, Application of 2-mercaptobenzothiazole self-assembled monolayer on polycrystalline gold electrode as a nanosensor for determination of Ag(I), Talanta 69 (2006) 741–746.

[51] S. Bharathi, V. Yegnaraman, G. P. Rao, Potential-dependent "opening" and "closing" of self-assembled 2-mercaptobenzthiazole on gold substrates, Langmuir 9 (1993) 1614–1617.

[52] H. Parham, N. Pourreza, F. Marahel, Resonance rayleigh scattering method for determination of 2-mercaptobenzothiazole using gold nanoparticles probe, Spectrochim. Acta A 151 (2015) 308–314.

[53] Z. Zhang, Q. Wang, X. Wang, L. Gao, The influence of crystal faces on corrosion behavior of copper surface: First-principle and experiment study, Appl. Surf. Sci. 396 (2017) 746–753.

[54] E. Vernack, D. Costa, P. Tingaut, P. Marcus, Theoretical studies of 2-mercaptobenzothiazole and 2-mercaptobenzimidazole as corrosion inhibitors for copper, submitted (2019).

[55] E. Protopopoff, P. Marcus, Potential–pH diagrams for hydroxyl and hydrogen adsorbed on a copper surface, Electrochim. Acta 51 (2005) 408–417.

[56] A. Gharachorlou, M. D. Detwiler, X.-K. Gu, L. Mayr, B. Klötzer, J. Greeley, R. G. Reifenberger, W. N. Delgass, F. H. Ribeiro, D. Y. Zemlyanov, Trimethylaluminum and oxygen atomic layer deposition on hydroxyl-free Cu(111), ACS Appl. Mater. Interfaces 7 (2015) 16428–16439.

[57] J.-H. Park, J.-H. Lee, A. Soon, Organics on oxidic metal surfaces: a first-principles DFT study of PMDA and ODA fragments on the pristine and mildly oxidized surfaces of Cu(111), Phys. Chem. Chem. Phys. 18 (2016) 21893.

[58] D. Gustinčič, A. Kokalj, DFT study of azole corrosion inhibitors on Cu_2O model of oxidized copper surfaces: I. Molecule–surface and Cl–surface bonding, Metals 8 (2018) 310.

[59] D. Gustinčič, A. Kokalj, DFT study of azole corrosion inhibitors on Cu_2O model of oxidized copper surfaces: II. Lateral interactions and thermodynamic stability, Metals 8 (2018) 311.

[60] A. Kokalj, D. Gustinčič, M. Poberžnik, M. Lozinšek, New insights into adsorption bonding of imidazole: A viable C2–H bond cleavage on copper surfaces, Appl. Surf. Sci. 479 (2019) 463–468.

[61] G. Sun, J. Kürti, P. Rajczy, M. Kertesz, J. Hafner, G. Kresse, Performance of the vienna ab initio simulation package (VASP) in chemical applications, J. Mol. Struct. THEOCHEM 624 (2003) 37–45.

[62] G. Kresse, J. Hafner, Phys. Rev. B 47 (1993) 558.

[63] G. Kresse, J. Furthmüller, Efficiency of ab-initio total energy calculations for metals and semiconductors using a plane-wave basis set, Comput. Mater. Sci 6 (1996) 15–50.

[64] G. Kresse, J. Furthmüller, Efficient iterative schemes for ab initio total-energy calculations using a plane-wave basis set, Phys. Rev. B 54 (1996) 11169–11186.

[65] G. Kresse, D. Joubert, From ultrasoft pseudopotentials to the projector augmented-wave method, Phys. Rev. B 59 (1999) 1758–1775.

[66] P. E. Blöchl, Projector augmented-wave method, Phys. Rev. B 50 (1994).

[67] J. P. Perdew, J. A. Chevary, S. H. Vosko, K. A. Jackson, M. R. Pederson, D. J. Singh, C. Fiolhais, Atoms , molecules , solids , and surfaces: Applications of the generalized gradient approximation for exchange and correlation, Phys. Rev. B 46 (1992).

[68] J. P. Perdew, K. Burke, M. Ernzerhof, Generalized gradient approximation made simple, Phys. Rev. Lett. 77 (1996).

[69] M. Methfessel, A. T. Paxton, High-precision sampling for Brillouin-zone integration in metals, Phys. Rev. B 40 (1989).

[70] H. J. Monkhorst, J. D. Pack, Special points for Brillonin-zone integrations, Phys. Rev. B 13 (1976).

[71] M. Dion, H. Rydberg, E. Schröder, D. C. Langreth, B. I. Lundqvist, Van der Waals density functional for general geometries, Phys. Rev. Lett. 92 (2004) 246401.

[72] J. Klimeŝ, D. R. Bowler, A. Michaelides, Chemical accuracy for the van der Waals density functional, J. Phys.: Condens. 22 (2010) 022201.

[73] J. Klimeš, D. R. Bowler, A. Michaelides, Van der Waals density functionals applied to solids, Phys. Rev. B 83 (2011) 195131.

[74] J. Klimeš, A. Michaelides, Perspective: Advances and challenges in treating van der Waals dispersion forces in density functional theory, J. Chem. Phys. 137 (2012) 120901.

[75] V. Maurice, H.-H. Strehlowa, P. Marcus, In situ STM study of the initial stages of oxidation of Cu(111) in aqueous solution, Surf. Sci. 458 (2000) 185–194.

[76] J. Kunze, V. Maurice, L. H. Klein, H.-H. Strehlowa, P. Marcus, In situ scanning tunneling microscopy study of the anodic oxidation of Cu(111) in 0.1 M NaOH, J. Phys. Chem. B 105 (2001) 4263–4269.

[77] J. Kunze, V. Maurice, L. H. Klein, H.-H. Strehlowa, P. Marcus, In situ STM study of the effect of chlorides on the initial stages of anodic oxidation of Cu(111) in alkaline solutions, Electrochim. Acta 48 (2003) 1157–1167.

[78] J. Kunze, V. Maurice, L. H. Klein, H.-H. Strehlowa, P. Marcus, In situ STM study of the duplex passive films formed on Cu(111) and Cu(001) in 0.1 M NaOH, Corros. Sci. 46 (2004) 245–264.

[79] P. Marcus, V. Maurice, Atomic level characterization in corrosion studies, Phil. Trans. R. Soc. A375 (2016) 20160414.

[80] H. P. Koch, Absorption spectra and structure of organic sulphur compounds., J. Chem. Soc. Part III (1949) 401–108.

[81] J. P. Chesick, J. Donohue, The molecular and crystal structure of 2-mercaptobenzothiazole, Acta Cryst. B 27 (1971) 1441–1444.

[82] A. K. Rai, R. Singh, K. N. Singh, V. B. Singh, FTIR, raman spectra and ab initio calculations of 2-mercaptobenzothiazole, Spectrochim. Acta A 63 (2006) 483–490.

[83] T. A. Mohamed, A. M. Mustafa, W. M. Zoghaib, M. S. Afifi, R. S. Farag, Y. Badr, Reinvestigation of benzothiazoline-2-thione and 2-mercaptobenzothiazole tautomers: Conformational stability, barriers to internal rotation and DFT calculations, J. Mol. Struct.: THEOCHEM 868 (2008) 27–36.

[84] W. Tang, E. Sanville, G. Henkelman, A grid-based bader analysis algorithm without lattice bias, J. Phys.: Condens. Matter 21 (2009) 084204.